Hyaluronic Acid Modified Covalent Organic Polymers for Efficient Targeted and Oxygen-Evolved Phototherapy

Fangpeng Shu
Guangzhou Medical University
Taowei Yang
Southern Medical University
Xuefeng Zhang
First Affiliated Hospital of Soochow University
Wenbin Chen
Southern Medical University
Kaihui Wu
Southern Medical University
Junqi Luo
Southern Medical University
Xumin Zhou
Southern Medical University
Guochang Liu
Guangzhou Medical University
Jianming Lu
Southern Medical University
Xiangming Mao (mxm631221@126.com)
Zhujiang Hospital of Southern Medical University https://orcid.org/0000-0002-7690-0924

Research

Keywords: Targeted therapy, photothermal therapy, photodynamic therapy, covalent organic polymers, hypoxia tumor

Posted Date: August 31st, 2020

DOI: https://doi.org/10.21203/rs.3.rs-62872/v1

Version of Record: A version of this preprint was published on January 6th, 2021. See the published version at https://doi.org/10.1186/s12951-020-00735-x.

Abstract

The integration of multiple functions with organic polymers-based nanoagent holds great potential to potentiate its therapeutic efficacy, but still remains challenges. In the present study, we design and prepare an organic nanoagent with oxygen-evolved and targeted ability for improved phototherapeutic efficacy. The iron ions doped poly diaminopyridine (FeD) is prepared by oxidize polymerization and modified with hyaluronic acid (HA). The obtained FeDH appears uniform morphology and size. Its excellent colloidal stability and biocompatibility are demonstrated. Specifically, the FeDH exhibits catalase-like activity in the presence of hydrogen peroxide. After loading of photosensitizer indocyanine green (ICG), the ICG@FeDH not only demonstrates favorable photothermal effect, but also shows improved generation ability of reactive oxygen species (ROS) under near-infrared laser irradiation. Moreover, the targeted uptake of ICG@FeDH in tumor cells is directly observed. As consequence, the superior phototherapeutic efficacy of the targeted ICG@FeDH over non-targeted counterparts is also confirmed in vitro and in vivo. Hence, the results demonstrate that the developed nanoagent rationally integrates the targeted ability, oxygen-evolved capacity and combined therapy in one system, offering a new paradigm of polymer-based nanomedicine for tumor therapy.

Introduction

Nanomaterials-enabled therapy provides unprecedented opportunities to increase the therapeutic efficacy and specificity of tumor treatments in the past decades [1–3]. Nanocarriers-based delivery system can effectively improve the tumor accumulation of drugs and reduces the undesirable side effects on normal tissues based on the enhanced permeability and retention (EPR) effect [4]. More importantly, various functional nanomaterials have been applied to mediate new alternatives for tumor treatment with lower side effects [5, 6]. Phototherapy, including photothermal and photodynamic therpay, has drawn widespread interest in recent years due to its minimal invasion and controllable spatiotemporal selectivity [7, 8]. In many previous studies, carbon- [9–11], semiconductor- [12–14], and metal-based nanomateirals [15–18] have been developed as photothermal agents for photothermal therpay of tumor. However, those inorganic nanomaterials are always debated with their biodegradability and long-term in vivo retention [19]. With regard to photodynamic therapy, the photosensitizers as small molecules are reqiured to be loaded into nanocarriers in order to prevent the photoblench process and improve the pharmacokinetics [20]. Therefore, the development of new type of nanocarriers is still urgently needed.

Covalent organic polymers, which are prepared by cross-linking organic molecules via covalent bonds, possess preferable stability under physiological conditions than traditional polymeric micelles and vesicles [21]. In several previous studies, covalent organic polymers have been demonstrated for chemo and phototherapy [22, 23]. However, as a newly emerged type of nanocarriers, covalent organic polymers still needs to be rationally functionalized for improved therapeutic efficacy. Liu’s group demonstrated nanoscale covalent organic polymers as a biodegradable nanomedicine for combined chemotherapy and photodynamic therapy [24, 25]. Porphyrinic covalent organic polymers have also been prepared for photothermal and photodynamic therapy [26]. Despite the excellent phototherapeutic efficacy, some

drawbacks should be conquered in the design of covalent organic polymer-based nanomedicine. For instance, the hypoxia condition in tumor microenvironment severely hinders the efficacy of oxygen-dependent photodynamic therapy and even causes drug resistance or tumor metastasis [27, 28]. Nanoenzyme, who can mimic the activity of natural catalase, has been widely integrated with nanoagents for oxygen-evolving therapy by catalyzing the decomposition of hydrogen peroxide in tumor microenvironment [29, 30]. Therefore, the fabrication of covalent organic polymers with catalase-like activity is worthwhile to realize more efficient phototherapy.

In this work, a covalent organic polymer-based nanoagent is developed for targeted and oxygen-evolving phototherapy of tumor. Specifically, nano-scaled polydiaminopyridine nanoparticles doped with iron ions (FeD) is prepared and conjugated with hyaluronic acid (HA), obtaining the designed nanoagent FeDH. With the loading of a photosensitive molecule indocyanine green (ICG), the ICG@FeDH holds potential to combine several advantages based on following considerations: first, the FeDH is constructed from organic molecules by strong covalent bonds, ensuring the excellent biocompatibility and colloidal stability under physiological condition; second, the iron ions can be doped into the nanoagent and render it with catalase-like activity, thereby overcoming the tumor hypoxia to improve the phototherapeutic efficacy. The iron ions might also facilitate the clearance of the developed nanoagent in comparison to other commonly used inorganic nanoenzyme, such as platinum [31], manganese dioxide [32] and other metal oxides [33, 34]. Last, the modification of HA endows FeDH with targeted ability towards tumor cells. Combining the catalase activity, photothermal and photodynamic effect of loaded ICG as well as the targeted ability of HA, the ICG@FeDH can realize more efficient phototherapeutic efficacy under near-infrared (NIR) laser irradiation.

Materials And Methods

Materials

2, 6-diaminopyridine, $FeCl_3$•$6H_2O$ and Sodium hyaluronate were commercially provided by Shanghai Aladdin Reagent CO, Ltd. (China). N-hydroxysuccinimide (NHS) and 1-(3-Dimethylaminopropyl)-3-ethylcarbodiimide hydrochloride (EDC·HCl) were brought from Sigma-Aldrich Trading Co., Ltd. (China). $[Ru(dpp)_3]Cl_2$ (RDPP), 1, 3-diphenylisobenzofuran (DPBF) and 2', 7'-dichlorofluorescein diacetate (DCFH-DA)were purchased from Shanghai Medpep Co., Ltd (China). Roswell Park Memorial Institute (RPMI) 1640, fetal bovine serum (FBS), penicillin–streptomycin, and trypsin were supplied by GIBCO Invitrogen Corp. (USA). Cell counting kit-8 (CCK-8) and 4',6-Diamidino-2-phenylindole (DAPI) were provided by Shanghai Yeasen Biotech Co., Ltd. (China). All other reagents were recieved and used without further purification. Deionized (DI) water was obtained from experimental water purification system .

Synthesis of FeD nanoparticles

In a 50 mL round-bottom flask, 8.0 mmol of $FeCl_3$•$6H_2O$ was stirred in 20 mL of deionized water for 0.5 h. Then, 2.0 mmol of 2, 6-diaminopyridine was added and the mixture was heated at 40 °C for 24 h. The

obtained FeD nanoparticles were collected by dialysis.

Preparation of FeDH

First, 0.1 g of HA, 36.2 mg of EDC and 27.9 mg of NHS were stirred in 10 mL of deionized water for 4 h. Then, 10 mL of FeD solutions (5 mg/mL) was added and reacted with activated HA for another 20 h. The HA modified FeD (denoted as FeDH) were obtained by high-speed centrifugation. To ICG-loaded FeDH (ICG@FeDH), 5 mg of ICG was added in FeD solutions and the modification is proceeded with the same steps. The samples were isolated and purified by centrifugation.

In vitro photothermal effect of ICG@FeDH

To evaluate the photothermal performance of ICG@FeDH, 0.5 mL of ICG@FeDH solution at different concentrations (100, 50, 25 μg/mL) was added into a Eppendorf tube (0.5 mL) and irradiated by the 808 nm laser (1 W/cm^2, 5 min). The temperature changes were timely measured by a infrared thermal imaging camera. As controls, the temperature of pure water or FeDH solution with concentration of 100 μg/mL were also recorded under the same conditions.

Assessment of oxygen generation ability

5 mL of H_2O_2 (2 mM) was mixed with 5 mL of FeDH dispersion with a dissolved oxygen meter inserted in the solution. The pure water and H_2O_2 solutions were also tested under the same conditions for comparison.

To evaluate the intracellular oxygen-evolving ability of FeDH, an oxygen-sensitive probe molecule RDPP was used to monitor the intracellular oxygen level. In brief, cells were seeded in culture dishes and then installed with RDPP (10 μM) at 37 °C for 2 h. Subsequently, the cells were treated with FeDH at 200 μg/mL for another 2 h. Finally, the human prostatic cancer cells (PC-3 cells) were rinsed with PBS for several times and directly imaged by confocal laser scanning microscope under an excitation of 488 nm.

Reactive oxygen species detection

Typically, DPBF was used as a probe molecule to detect the singlet oxygen generation of different samples [35]. 1 mL of ICG@FeDH aqueous solution at concentration of 100 μg/mL was mixed with 50 μL of DPBF dissolved in dimethyl sulfoxide (10 mM) and irradiated by a 808 nm laser (1 mW/cm^2). The absorbance at 419 nm was measured by a UV-vis spectrophotometer at different time intervals.

To investigate the intracellular ROS generation, PC-3 cells were seeded in culture dishes and incubated with ICG@FeDH (50 μg/mL) for 4 h. Then the cells were incubated with DCFH-DA (2 μM) for 0.5 h. After removing the excess probe, the cells were further illuminated by 808 nm laser for 10 min, and imaged by CLSM under the excitation of 808 nm. The cells treated with complete medium alone, laser irradiation alone, and ICG@FeDH alone were also stained with DCFH-DA for control. Moreover, the cells pre-treated

with HA were also set as the receptor-inhibition group, in which the same protocol was performed except that the PC-3 cells were pre-treated with free HA (5 mg/mL) for 2 h before the incubation and irradiation.

Targeted ability of ICG@FeDH

Targeted ability of ICG@FeDH was also investigated by CLSM. Typically, PC-3 cells were seeded in culture dish at density of 2×10^5 cells/dish for 24 h. Subsequently, the cells were cultured with ICG@FeD and ICG@FeDH for 2 h. After removing the medium, the cells were washed, fixed by 4% paraformaldehyde and imaged by CLSM under oil lens. Moreover, the cells pre-treated with free HA were also incubated with ICG@FeDH and observed by CLSM. The cells without treatments were set as control.

In vitro cytotoxicity and cell killing effect

The cytotoxicity of free FeDH was assessed by standard CCK-8 assay. In a typical process, PC-3 cells were seeded into 96-well plates at a density of 1×10^4 cells/well for 24 h. Then the medium was replaced with different concentrations of FeDH, and the cells were further incubated for another 24 h. After that, the cells were rinsed with PBS. After 4 h incubation, the medium was replaced with CCK-8 work solution and incubated at 37 °C for 2 h. The absorbance at 450 nm of each well was measured by a microplate reader. The cell viability was calculated by the value of the control group divided by the values of the samples [36]. Four parallel experiments were set for each sample.

To evaluate the cancer cell killing effect, PC-3 cells were seeded into 96-well plates at a density of 1×10^4 cells/well for 24 h, and further incubated with ICG@FeDH (100 μg/mL) for 4 h. Then the cells were irradiated by 808 nm laser for 10 min, followed by incubated at 37 °C for another 20 h. For comparison, the cells treated with complete medium, NIR laser alone, ICG@FeDH alone, and ICG@FeDH + NIR laser with the pre-treatment of free HA were set as different groups with corresponding procedures. Last, the cell viability was evaluated by CCK-8 assay as described above.

In vivo antitumor effect

All animal experiments were approved by the Animal Care and Use Committee of Southern Medical University, Guangzhou, China. 4-6 weeks-old male nude Balb/c mice were provided by Experimental Animal Center of Southern Medical University. The tumor model was established by subcutaneously injecting PC-3 cells (2×10^6 cells) into right back of the mice. After the tumor size reached ~50 mm^3, the tumor-bearing mice were randomly divided into four groups (n = 4): PBS (control group), NIR laser alone (irradiation group), ICG@FeD with laser irradiation (non-targeted group) and ICG@FeDH with laser irradiation (targeted group). Correspondingly, the experimental mice were intravenously injected with different samples (4 mg/mL, 0.2 mL). For irradiation groups, the tumor site of mice was exposed to 808 nm laser for 10 min. The treatments were performed day 1 and day 3. After that, the tumor size and body weight of experimental mice were monitored every two days. Moreover, the tumors of each group were extracted for hematoxylin&eosin and immunofluorescent staining.

Statistical analysis

The results were expressed as mean ± standard deviation. The significance was analyzed by one-way analysis of variance (ANOVA) statistical method and Scheffe's post hoc test. The criteria was set as *p < 0.05 and **p < 0.01 for statistical significance.

Results And Discussion

Synthesis and characterization of FeDH

As depicted in **Scheme 1**, the FeD was first prepared by iron ions-initiated polymerization of DAP monomer [37]. TEM images show that as-prepared FeD nanoparticles exhibit fusiform-like structure with a length of 72 nm and width of 20 nm (**Figure 1A**). The porosity of FeD nanoparticles can be clearly seen in high-magnification TEM image. Moreover, SEM image demonstrate the uniform morphology of FeD in large scale (**Figure 1C**). Due to the abundant amino groups on FeD, the targeted molecule HA can be modified onto it by amide reaction. The obtained FeDH maintains the original structure, and the pores are still visible in TEM image (**Figure 1D-F**). Further, the element mapping of FeDH is recorded on scanning TEM. Notably, strong signals from iron element can be observed, the energy dispersive X-ray spectrum also confirms the existence of iron ions in FeDH (**Figure 1G-H**). It has been reported the iron ions (Fe^{3+}) can react with hydrogen peroxide by Fention-like reaction [38, 39], modulating the tumor microenvironment and producing sufficient oxygen to enhance the therapeutic efficacy. Thus, ICG is selected as photosensitizers to be loaded in FeDH. Accordingly, the typical absorption peak of ICG at NIR region for ICG@FeDH verifies the efficient loading process (**Figure 1I**). Additionally, the zeta potential of prepared samples is also measured. The bare FeD displays strong positive surface due to the amino groups of DAP (**Figure 1J**). Zeta potential of FeDH turns to -20.3 mV after modification of HA and the ICG@FeDH also exhibits negative surface, which is expected to benefit the colloidal stability of nanoparticles [40]. Then the colloidal stability of FeDH is inspected by DLS. As expected, the size distribution of FeDH in different media, including water, PBS and cell culture medium, shows no abnormality but slight increase in PBS and cell medium (**Figure 1K**). Moreover, the average size of FeDH exhibits no obvious change in one week, and no agglomeration appears after one week storage (**Figure 1L**), suggesting the excellent colloidal stability of FeDH.

Photothermal effect of ICG@FeDH

Since the ICG@FeDH shows strong NIR absorption, its photothermal property is evaluated next. First, the ICG@FeDH solutions with different concentrations were irradiated with 808 nm laser for 5 min. The temperature of the solutions exhibit an obvious concentration-dependent increase (**Figure 2A**), which gradually elevates to 42.3 °C at a low concentration of 100 μg/mL and power density of 1.0 W/cm^{-2}. However, the temperature of free FeDH solutions changes 1.2 °C after 5 min of irradiation, and the pure water only 0.3 °C under the same conditions (**Figure 2B and C**). The strong contrast of pseudo-color in thermal imaging photos also demonstrates the superior photothermal effect of ICG@FeDH than that of

free FeDH (**Figure 2D**). Therefore, the results confirm that the loading of ICG into FeDH makes it become an excellent photothermal agent.

In vitro photodynamic effect of ICG@FeDH

In addition to the enhanced photothermal effect, ICG can also generate singlet oxygen under NIR laser irradiation [41]. Thus, the photodynamic effect of ICG@FeDH is investigated. On the other hand, the doped iron ions of FeDH can catalyze the decomposition of hydrogen peroxide. The oxygen level of FeDH solution rapidly increases with the addition of hydrogen peroxide, while the pure water or hydrogen peroxide alone cannot produce oxygen under the same conditions (**Figure 3A**). The catalase-like activity of FeDH is further confirmed in living cells by a commercial O_2 sensing probe RDPP [42]. No surprisingly, the green fluorescence of RDPP in cells treated with FeDH was dramatically weakened as compared to the cells without treatments (**Figure 3B**). The result evidences that iron ions doped in FeDH can efficiently catalyze the decomposition of hydrogen peroxide to generate intracellular oxygen, thereby relieving the hypoxia condition in tumor microenvironment. Based on this, the photodynamic effect of ICG@FeDH is also expected to be improved due to the elevated oxygen level. To illustrate this issue, another probe DPBF is used to evaluate the singlet oxygen generation ability of ICG@FeDH under excitation of NIR laser. As expected, the absorption peak of DPBF decreases with the irradiation time of NIR laser (**Figure 3C**), implying the generation of singlet oxygen. Moreover, the decrease of the absorption value becomes faster when hydrogen peroxide is added into the ICG@FeDH solution (**Figure 3D**). Specifically, after 5 min irradiation, 64.8% of DPBF is oxidized in the presence of hydrogen peroxide (**Figure 3E**), which is much high than that of ICG@FeDH alone (57%), suggesting that the oxygen-evolving capacity of FeDH.

Targeted ability of ICG@FeDH

With specific affinity towards CD44-receptor [43, 44], the attachment of HA on FeDH can render it with targeted ability towards tumor cells. To demonstrate this, the intracellular uptake of ICG@FeDH is investigated by CLSM using PC-3 cells. After the cells were co-incubated with ICG loaded nanoparticles for 4 h, the red fluorescence of ICG is very weak for non-targeted ICG@FeD. In sharp contrast, strong red fluorescence can be observed around the nucleus for ICG@FeDH group (**Figure 4**), which can be attributed to the specific binding of HA with CD44 receptors on PC-3 cells. Once the receptors are inhibited by treating PC-3 cells with free HA, the intracellular fluorescent intensity for ICG@FeDH obviously decreases, further confirming the receptor-mediated endocytosis of ICG@FeDH. Taken together, the modification of HA endows FeDH with excellent targeted ability for tumor therapy.

In vitro evaluation of ICG@FeDH

Next, the tumor cell killing effect of ICG@FeDH is assessed using PC-3 cells. With the aforementioned photothermal and photodynamic effect, ICG@FeDH is supposed to exert favorable killing effect on tumor cells under NIR laser irradiation. DCFH-DA, a probe molecule that can be oxidized to emit fluorescence at 488 nm [45], is applied to assess the cellular amount of reactive oxygen species (ROS), the major killing mechanism of photodynamic therapy. As shown in **Figure 5A**, the cells treated with laser irradiation or

ICG@FeDH alone display very weak fluorescence, while the bright green fluorescence can be observed upon laser irradiation for both ICG@FeD and ICG@FeDH treated cells. In particular, the fluorescent intensity of ICG@FeDH with laser irradiation is determined to be 108.3 (**Figure 5B**), which is much stronger than that of ICG@FeH with laser irradiation (~75.4), demonstrating the higher ROS level for ICG@FeDH. The result can be ascribed to the enhanced cellular uptake of targeted ICG@FeDH as mentioned above.

To further evaluate the cell killing efficacy, the cytotoxicity of free FeDH is investigated first. The result of CCK-8 demonstrates that the cells treated with various concentrations of FeDH all show negligible toxicity even at a ultra-high concentration of 1600 μg/mL, suggesting the outstanding biocompatibility of FeDH. Thus, this polymer-based nanocarrier is highly suitable for biological applications in comparison to those non-degradable inorganic nanomaterials [46]. Afterwards, the killing effect is assessed using PC-3 cells. As expected, cells treated with ICG@FeDH or laser irradiation alone exhibit high cell viability over 95%. In sharp contrast, upon laser irradiation, cell mortality is significantly increased in the group of ICG@FeDH than in ICG@FeD. The superior cell killing efficacy of ICG@FeDH is probably due to its excellent photothermal and photodynamic effect under laser irradiation. Combining with the modification of HA, the ICG@FeDH can serve as a targeted phototherapeutic agent for killing tumor cells.

In vivo antitumor effect of ICG@FeDH

Next, the in vivo therapeutic efficacy of ICG@FeDH was investigated on PC-3 tumor-bearing mice. To implement the treatments, the mice are intravenously injected with ICG@FeDH and NIR laser irradiation is conducted. **Figure 6A** shows the variation of relative tumor volume in the period of treatment. The tumors treated by ICG@FeDH with 808 nm laser irradiation were remarkably inhibited and displayed a relative tumor volume of 0.38 on day 6 without any recurrence, implying the superior phototherapeutic efficacy of ICG@FeDH under NIR laser irradiation. As for control groups of PBS and NIR laser alone, the size of tumors are rapidly increased within two weeks, showing negligible therapeutic effect. Notably, the ICG@FeD with laser irradiation shows an inferior tumor inhibition rate in comparison to the counterpart of ICG@FeDH, which confirms that the modification of HA can improve its in vivo antitumor effect. Besides, the body weight of experimental mice shows no obvious change in the period of treatments (**Figure 6B**), indicating that the well-tolerance and excellent biocompatibility of the applied samples. Furthermore, the tumors are harvested at the end of treatments and stained with H&E for histological analysis. The images show that no apparent necrosis appears in control group (**Figure 6C**). Moreover, the group of ICG@FeDH plus laser irradiation exhibits much more necrosis and karyolysis in slice than that in the group of non-targeted ICG@FeD plus laser irradiation. It is deduced that the better therapeutic efficacy of ICG@FeDH is mainly resulted from targeted ability of HA as well as the improved photodynamic effect because of the oxygen-evolved capacity of FeDH. To better understand this, the immunofluorescent staining of hypoxia-inducible factor 1α (HIF1-α) is conducted to detect the oxygen level in tumor. The green fluorescence indicative of hypoxia remarkably reduces in the group of ICG@FeDH (**Figure 6D**). It should be noticed that the fluorescence in the group of ICG@FeD is also weakened as compared with control group and NIR laser group, but still stronger than ICG@FeDH, which is probably due to that the efficient targeted ability

of ICG@FeDH render it with higher accumulation at tumor site. Taken together, ICG@FeDH effectively integrates several advantages, including excellent biocompatibility and targeted ability as well as oxygen-evolved capacity for enhanced phototherapeutic efficacy, showing great potential for biomedical applications.

Conclusion

In summary, a new type of polymer-based nanocarrier is fabricated by oxidize polymerization for efficiently targeted and oxygen-evolved phototherapy of tumor. The synthesized FeD shows fusiform-like structure with average size of ~ 70 nm. With the surface modification of HA, the obtained FeDH not only possesses outstanding colloidal stability and excellent biocompatibility for biomedical application. More importantly, the doped iron ions in FeDH are demonstrated with catalase-like activity, which can catalyze the generation of oxygen in hydrogen peroxide-excessive tumor microenvironment. After loading the photosensitizer ICG into FeDH, the obtained FeDH demonstrates favorable photothermal effect, enhanced photodynamic effect and specific binding affinity towards PC-3 tumor cells, achieving efficiently targeted and combined phototherapy of tumor in vitro and in vivo. Overall, this simple but efficient nanoagent provides a new paradigm of polymer-based nanocarrier for enhanced phototherapeutic efficacy.

Declarations

Acknowledgement

This work was supported by the National Natural Science Foundation of China (No.81773277) and Science and Technology Program of Guangzhou (No.201803010014).

Ethics approval and consent to participate

All animal experiments were approved by the Animal Care and Use Committee of Southern Medical University, Guangzhou, China.

Consent for publication

All authors consent the publication of this manuscript.

Availability of data and material

All data discussed in this study are presented in the current manuscript.

Competing interests

The authors declare no competing interests.

Funding

The authors acknowledge the financial support from the National Natural Science Foundation of China (No.81773277) and Science and Technology Program of Guangzhou (No.201803010014).

Authors' contributions

S. Fang and X. Mao designed organized this work. S. Fang and T. Yang performed the experiments and analyzed the data. X. Zhang, W. Chen, K. Wu, J. Luo, and X, Zhou assisted S. Fang and T. Wang for the data collection and biological experiments. S. Fang, G. Liu, J. Lu and X. Mao wrote the manuscript. All authors contributed to the discussion and edits the final version of the manuscript.

References

1. Stuart M A C, Huck W T S, Genzer J, Muller M, Ober C, Stamm M, et al. Emerging applications of stimuli-responsive polymer materials. Nat. Mater. 2010;9(2):101-13.
2. Mura S, Nicolas J, Couvreur P. Stimuli-responsive nanocarriers for drug delivery. Nat. Mater. 2013;12(11):991-1003.
3. Shi J J, Kantoff P W, Wooster R, Farokhzad O C. Cancer nanomedicine: Progress, challenges and opportunities. Nat. Rev. Cancer. 2017;17(1):20-37.
4. Youn Y S, Bae Y H. Perspectives on the past, present, and future of cancer nanomedicine. Adv. Drug. Deliver. Rev. 2018;130:3-11.
5. Russell L M, Liu C H, Grodzinski P. Nanomaterials innovation as an enabler for effective cancer interventions. Biomaterials. 2020;242.
6. Liu Y Y, Jiang Y Q, Zhang M, Tang Z M, He M Y, Bu W B. Modulating hypoxia via nanomaterials chemistry for efficient treatment of solid tumors. Acc. Chem. Res. 2018;51(10):2502-11.
7. Liu Y J, Bhattarai P, Dai Z F, Chen X Y. Photothermal therapy and photoacoustic imaging via nanotheranostics in fighting cancer. Chem. Soc. Rev. 2019;48(7):2053-108.
8. Zhou Z J, Song J B, Nie L M, Chen X Y. Reactive oxygen species generating systems meeting challenges of photodynamic cancer therapy. Chem. Soc. Rev. 2016;45(23):6597-626.
9. Yang K, Zhang S A, Zhang G X, Sun X M, Lee S T, Liu Z A. Graphene in mice: Ultrahigh in vivo tumor uptake and efficient photothermal therapy. Nano. Lett. 2010;10(9):3318-23.
10. Meng Y, Wang S S, Li C Y, Qian M, Yan X Y, Yao S C, et al. Photothermal combined gene therapy achieved by polyethyleneimine-grafted oxidized mesoporous carbon nanospheres. Biomaterials. 2016;100:134-42.
11. Wang S H, Shang L, Li L L, Yu Y J, Chi C W, Wang K, et al. Metal-organic-framework-derived mesoporous carbon nanospheres containing porphyrin-like metal centers for conformal phototherapy. Adv. Mater.2016;28(38):8379-87.
12. Yang W T, Guo W S, Le W J, Lv G X, Zhang F H, Shi L, et al. Albumin-bioinspired Gd:CuS nanotheranostic agent for in vivo photoacoustic/magnetic resonance imaging-guided tumor-targeted photothermal therapy. ACS Nano. 2016;10(11):10245-57.

13. Yu W J, Yu N, Wang Z J, Li X, Song C, Jiang R Q, et al. Chitosan-mediated green synthesis and folic-acid modification of CuS quantum dots for photoacoustic imaging guided photothermal therapy of tumor. J. Colloid Interface Sci. 2019;555:480-88.
14. Wang K, Zhuang J L, Liu Y B, Xu M S, Zhuang J Y, Chen Z G, et al. PEGylated chitosan nanoparticles with embedded bismuth sulfide for dual-wavelength fluorescent imaging and photothermal therapy. Carbohydr. Polym. 2018;184:445-52.
15. Zhang L, Yang X Q, Wei J S, Li X, Wang H, Zhao Y D. Intelligent gold nanostars for in vivo CT imaging and catalase-enhanced synergistic photodynamic & photothermal tumor therapy. Theranostics. 2019;9(19):5424-42.
16. Du Y, Jiang Q, Beziere N, Song L L, Zhang Q, Peng D, et al. DNA-nanostructure-gold-nanorod hybrids for enhanced in vivo optoacoustic imaging and photothermal therapy. Adv. Mater. 2016;28(45):10000-07.
17. Lei P P, An R, Zhang P, Yao S, Song S Y, Dong L L, et al. Ultrafast synthesis of ultrasmall poly(vinylpyrrolidone)-protected bismuth nanodots as a multifunctional theranostic agent for in vivo dual-modal CT/photothermal-imaging-guided photothermal therapy. Adv. Funct. Mater. 2017;27(35):201702018.
18. Chen T, Cen D, Ren Z H, Wang Y F, Cai X J, Huang J, et al. Bismuth embedded silica nanoparticles loaded with autophagy suppressant to promote photothermal therapy. Biomaterials, 2019;221:119419.
19. Yang G B, Phua S Z F, Bindra A K, Zhao Y L. Degradability and clearance of inorganic nanoparticles for biomedical applications. Adv. Mater. 2019;31(10):201805730.
20. Sztandera K, Gorzkiewicz M, Klajnert-Maculewicz B. Nanocarriers in photodynamic therapy-in vitro and in vivo studies. Wiley Interdiscip. Rev.: Nanomed. Nanobiotechnol. 2020;12(3):1599.
21. Ding S Y, Wang W. Covalent organic frameworks (COFs): From design to applications. Chem. Soc. Rev. 2013;42(2):548-68.
22. Tao D L, Feng L Z, Chao Y, Liang C, Song X J, Wang H R, et al. Covalent organic polymers based on fluorinated porphyrin as oxygen nanoshuttles for tumor hypoxia relief and enhanced photodynamic therapy. Adv. Funct. Mater. 2018;28(43):201804901.
23. Tan J, Namuangruk S, Kong W F, Kungwan N, Guo J, Wang C C. Manipulation of amorphous-to-crystalline transformation: Towards the construction of covalent organic framework hybrid microspheres with NIR photothermal conversion ability. Angew. Chem., Int. Ed. 2016;55(45):13979-84.
24. Wang H R, Zhu W W, Feng L Z, Chen Q, Chao Y, Dong Z L, et al. Nanoscale covalent organic polymers as a biodegradable nanomedicine for chemotherapy-enhanced photodynamic therapy of cancer. Nano Res. 2018;11(6):3244-57.
25. Wang H R, Zhu W W, Liu J J, Dong Z L, Liu Z. pH-responsive nanoscale covalent organic polymers as a biodegradable drug carrier for combined photodynamic chemotherapy of cancer. ACS Appl. Mater. Interfaces. 2018;10(17):14475-82.

26. Shi Y S, Liu S N, Liu Y, Sun C Q, Chang M Y, Zhao X Y, et al. Facile fabrication of nanoscale porphyrinic covalent organic polymers for combined photodynamic and photothermal cancer therapy. ACS Appl. Mater. Interfaces. 2019;11(13):12321-26.
27. Li M L, Shao Y J, Kim J H, Pu Z J, Zhao X Z, Huang H Q, et al. Unimolecular photodynamic O_2-economizer to overcome hypoxia resistance in phototherapeutics. J. Am. Chem. Soc. 2020;142(11):5380-88.
28. He Y C, Cong C, He Y Q, Hao Z N, Li C H, Wang S, et al. Tumor hypoxia relief overcomes multidrug resistance and immune inhibition for self-enhanced photodynamic therapy. Chem. Eng. J. 2019;375:122079.
29. Li X S, Kwon N, Guo T, Liu Z, Yoon J. Innovative strategies for hypoxic-tumor photodynamic therapy. Angew. Chem., Int. Ed. 2018;57(36):11522-31.
30. Li Y H, Jian X X, Zhou S S, Lu Y X, Zhao C X, Gao Z D, et al. Protein shell-encapsulated pt clusters as continuous O_2-supplied biocoats for photodynamic therapy in hypoxic cancer cells. ACS Appl. Mater. Interfaces. 2019;11(19):17215-25.
31. Zhang Y, Wang F M, Liu C Q, Wang Z Z, Kang L H, Huang Y Y, et al. Nanozyme decorated metal-organic frameworks for enhanced photodynamic therapy. ACS Nano. 2018;12(1):651-61.
32. Lin T S, Zhao X Z, Zhao S, Yu H, Cao W M, Chen W, et al. O_2-generating MnO_2 nanoparticles for enhanced photodynamic therapy of bladder cancer by ameliorating hypoxia. Theranostics. 2018;8(4):990-1004.
33. Zhen W Y, Liu Y, Lin L, Bai J, Jia X D, Tian H Y, et al. BSA-IrO_2: Catalase-like nanoparticles with high photothermal conversion efficiency and a high X-ray absorption coefficient for anti-inflammation and antitumor theranostics. Angew. Chem., Int. Ed. 2018;57(32):10309-13.
34. Zhen W Y, Liu Y, Wang W, Zhang M C, Hu W X, Jia X D, et al. Specific "unlocking" of a nanozyme-based butterfly effect to break the evolutionary fitness of chaotic tumors. Angew. Chem., Int. Ed. 2020;59(24):9491-97.
35. Cheng Y, Kong X P, Chang Y, Feng Y L, Zheng R X, Wu X Q, et al. Spatiotemporally synchronous oxygen self-supply and reactive oxygen species production on z-scheme heterostructures for hypoxic tumor therapy. Adv. Mater. 2020;32(11):201908109.
36. Shu F P, Lv D J, Song X L, Huang B, Wang C, Yu Y Z, et al. Fabrication of a hyaluronic acid conjugated metal organic framework for targeted drug delivery and magnetic resonance imaging. RSC. Adv. 2018;8(12):6581-89.
37. Bai J, Jia X D, Zhen W Y, Cheng W L, Jiang X. A facile ion-doping strategy to regulate tumor microenvironments for enhanced multimodal tumor theranostics. J. Am. Chem. Soc. 2018;140(1):106-09.
38. Yang Y, Zhu W J, Feng L Z, Chao Y, Yi X, Dong Z L, et al. G-quadruplex-based nanoscale coordination polymers to modulate tumor hypoxia and achieve nuclear-targeted drug delivery for enhanced photodynamic therapy. Nano. Lett. 2018;18(11):6867-75.

39. Wu X, Yan P J, Ren Z H, Wang Y F, Cai X J, Li X, et al. Ferric hydroxide-modified upconversion nanoparticles for 808 nm NIR-triggered synergetic tumor therapy with hypoxia modulation. ACS Appl. Mater. Interfaces. 2019;11(1):385-93.
40. Sun Q H, Zhou Z X, Qiu N S, Shen Y Q. Rational design of cancer nanomedicine: Nanoproperty integration and synchronization. Adv. Mater. 2017;29(14):201606628.
41. Ren S S, Cheng X, Chen M K, Liu C, Zhao P C, Huang W, et al. Hypotoxic and rapidly metabolic PEG-PCL-C3-ICG nanoparticles for fluorescence-guided photothermal/photodynamic therapy against OSCC. ACS Appl. Mater. Interfaces. 2017;9(37):31509-18.
42. He Z M, Xiao Y, Zhang J R, Zhang P H, Zhu J J. In situ formation of large pore silica-MnO_2 nanocomposites with H^+/H_2O_2 sensitivity for O_2-elevated photodynamic therapy and potential mr imaging. Chem. Commun. 2018;54(24):2962-65.
43. Huang L, Ao L J, Wang W, Hu D H, Sheng Z H, Su W. Multifunctional magnetic silica nanotubes for MR imaging and targeted drug delivery. Chem. Commun. 2015;51(18):3923-26.
44. Lima-Sousa R, de Melo-Diogo D, Alves C G, Costa E C, Ferreira P, Louro R O, et al. Hyaluronic acid functionalized green reduced graphene oxide for targeted cancer photothermal therapy. Carbohydr. Polym. 2018;200:93-99.
45. Zheng X H, Wang L, Pei Q, He S S, Liu S, Xie Z G. Metal-organic framework@porous organic polymer nanocomposite for photodynamic therapy. Chem. Mater. 2017;29(5):2374-81.
46. Ju Y M, Dong B, Yu J, Hou Y L. Inherent multifunctional inorganic nanomaterials for imaging-guided cancer therapy. Nano Today. 2019;26:108-22.

Figures

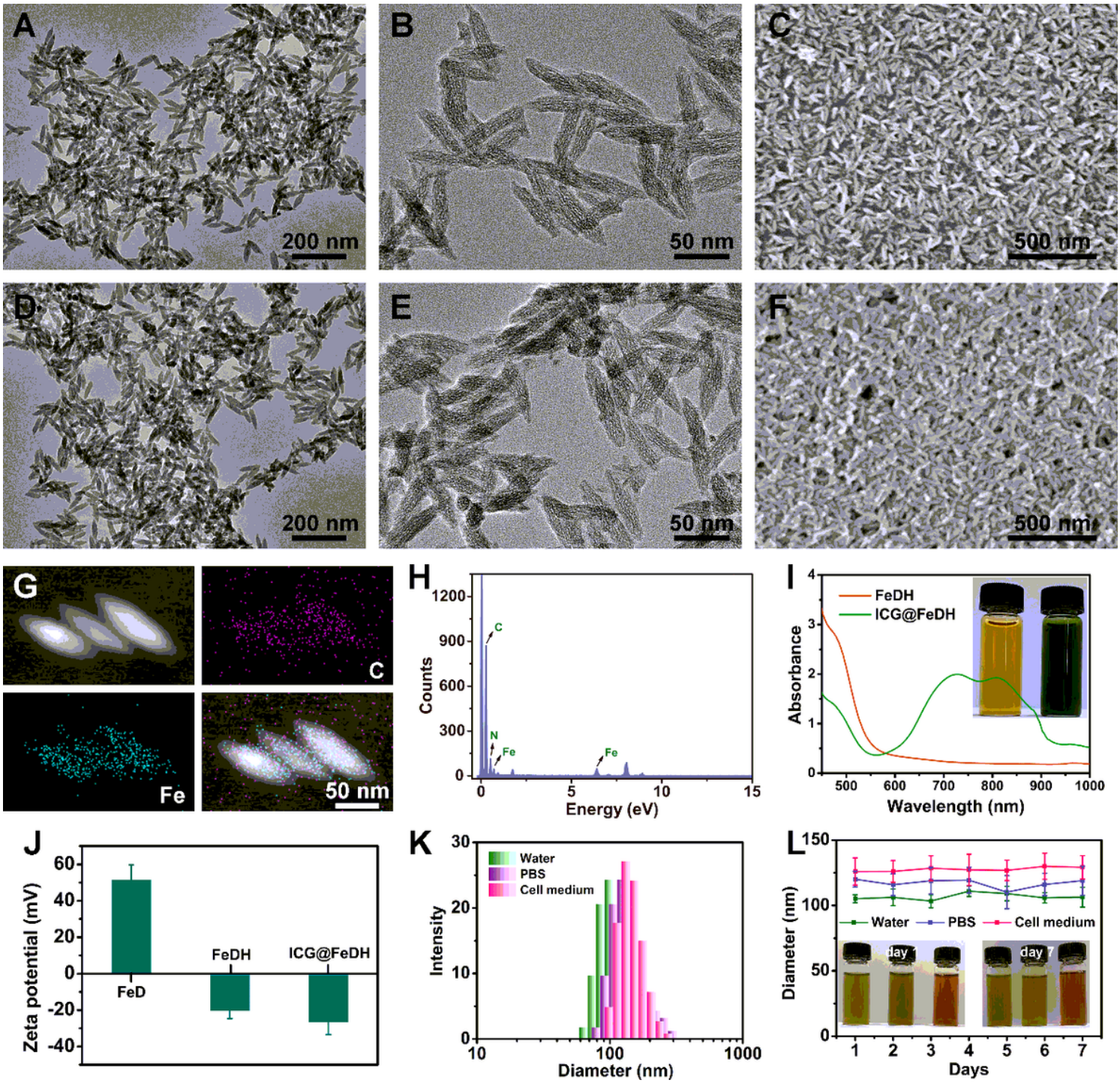

Figure 1

Transmission electron microscopy (TEM) images of (A-B) FeD and (D-E) FeDH. Scanning electron microscopy (SEM) images of (C) FeD and (F) FeDH. (G) High-angle annular dark field scanning TEM (HAADF-STEM) image and element mapping of FeDH. (H) Energy dispersive X-ray spectrum of FeDH. (I) UV-vis spectra of FeDH and ICG@FeDH. (J) Zeta potential results of different samples. (K) Size distributions of FeDH dispersed in different media. (L) Average size of FeDH in different media measured by dynamic light scattering (DLS) within one week.

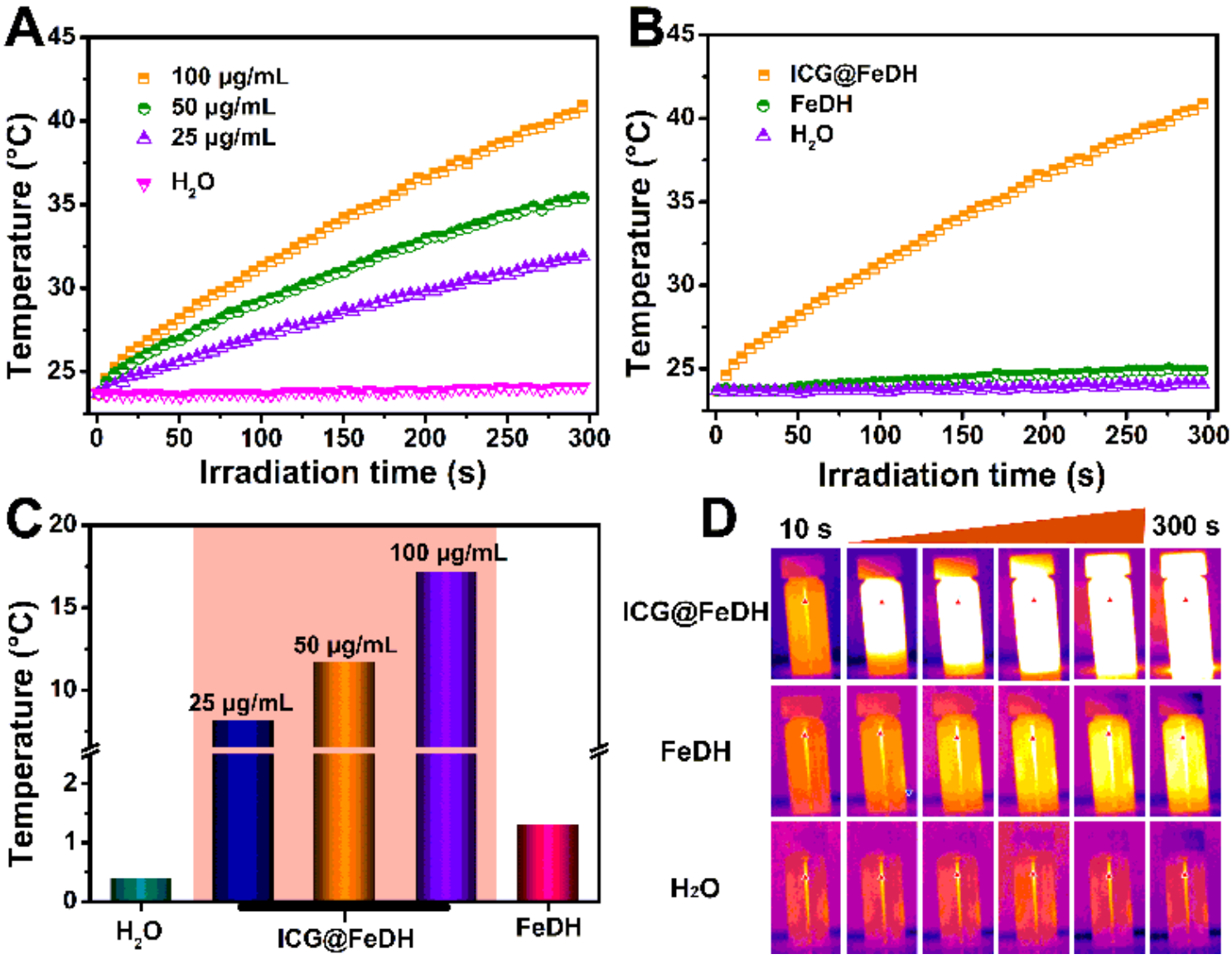

Figure 2

(A) The temperature change versus irradiation time of FeDH aqueous dispersions at different concentrations. Curves. (B) The heating curve of ICG@FeDH, FeDH and H2O under the same conditions (1 W/cm2, 5 min). (C) Temperature change value and (D) thermal imaging photos at different time points of the corresponded samples in B.

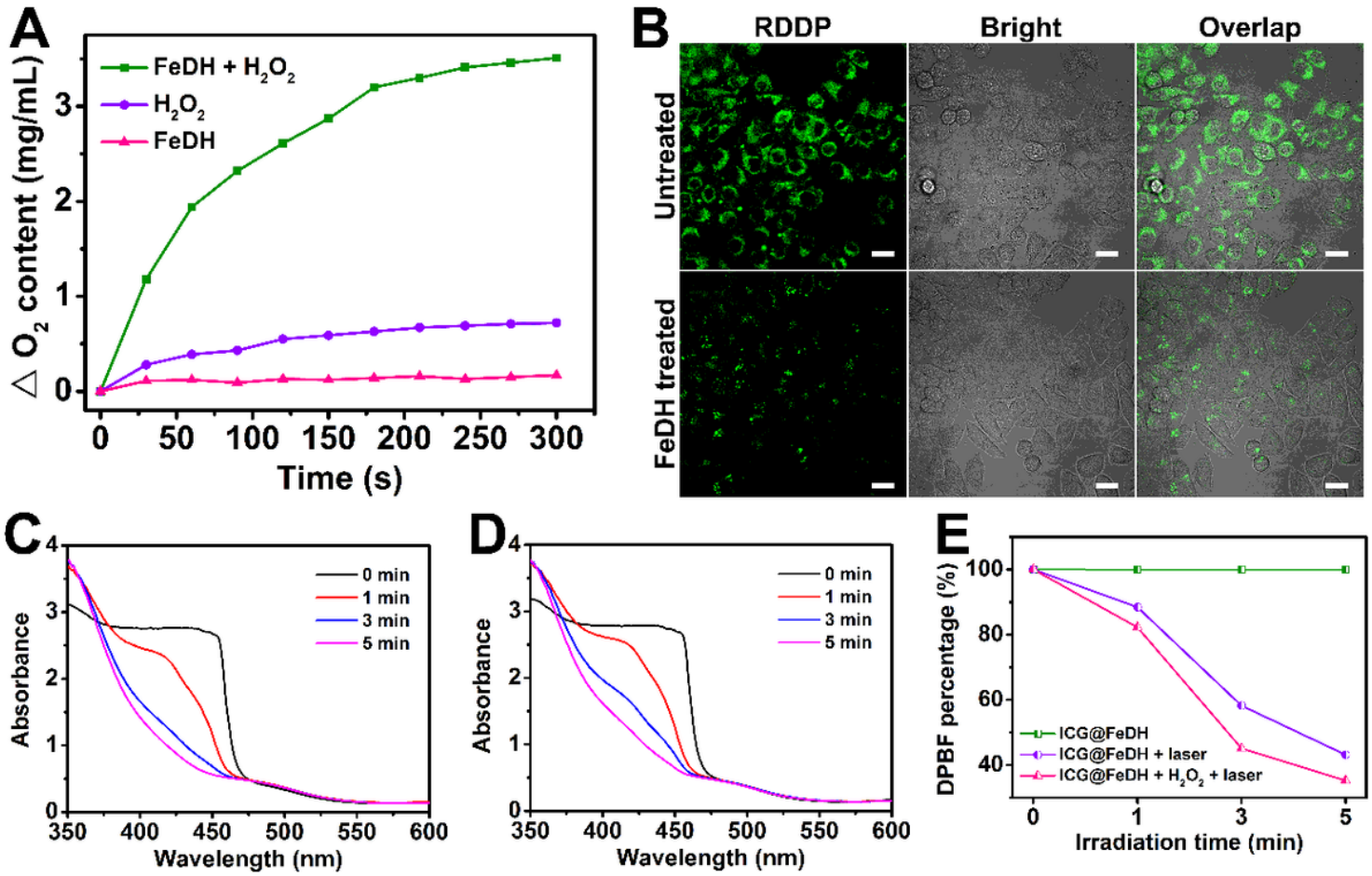

Figure 3

(A) The oxygen content of different samples measured by digital oxygen meter. (B) Confocal laser scanning microscopy (CLSM) images of PC-3 cells after stained with RDDP for 2 h and incubated with or without FeDH for another 2 h. (C) UV-vis spectra of DPBF solutions mixed with (C) ICG@FeDH plus hydrogen peroxide and (D) ICG@FeDH under 808 nm laser irradiation for different time points. (E) The calculated degradation rate of DPBF based on the absorbance values at 419 nm in C and D.

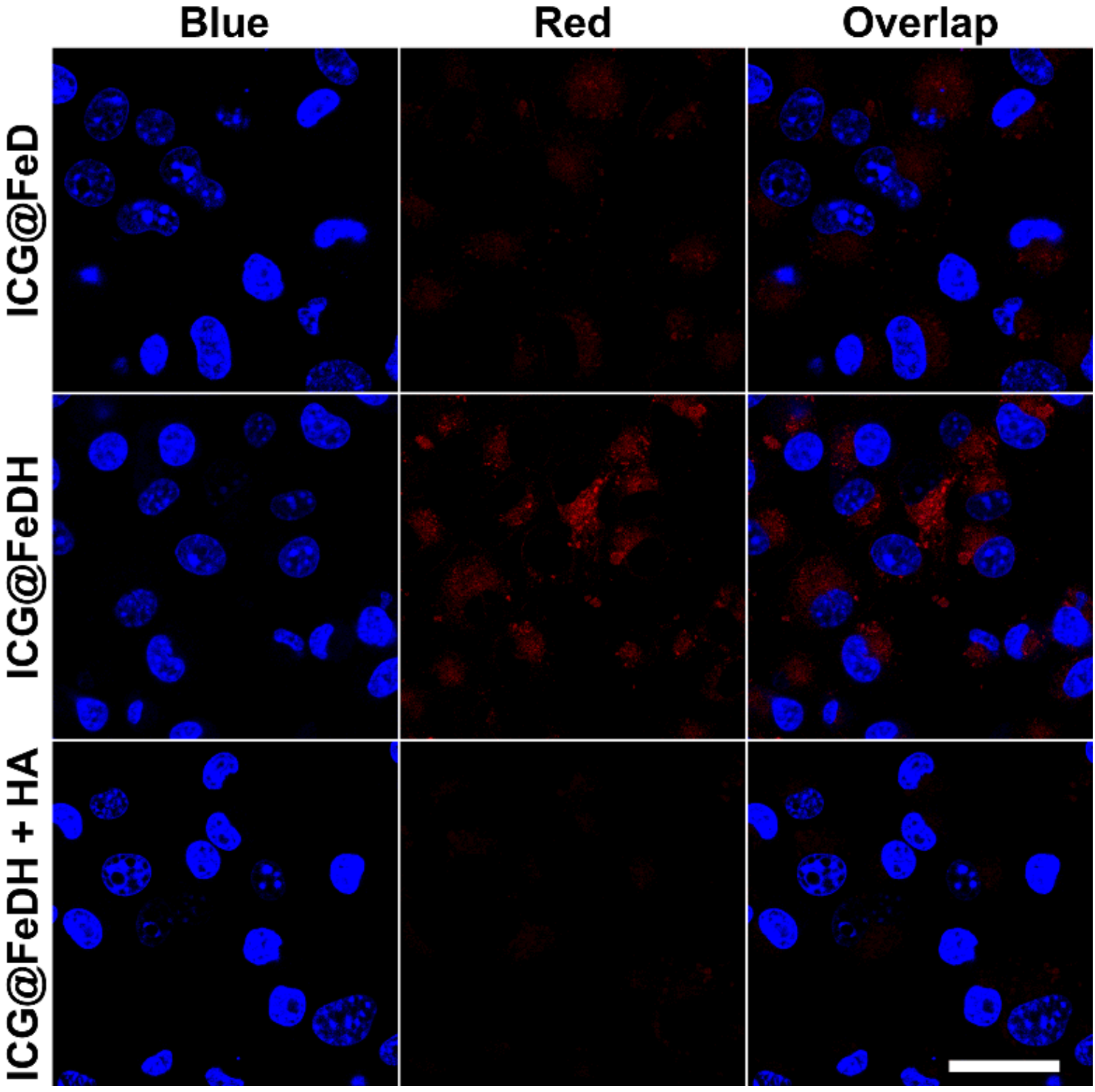

Figure 4

CLSM images of PC-3 cells treated with ICG@FeD, ICG@FeDH and ICG@FeDH with free HA pre-treatment for 2 h. Blue color represents DAPI, red color represents the fluorescence of ICG. Scle bar is 40 μm.

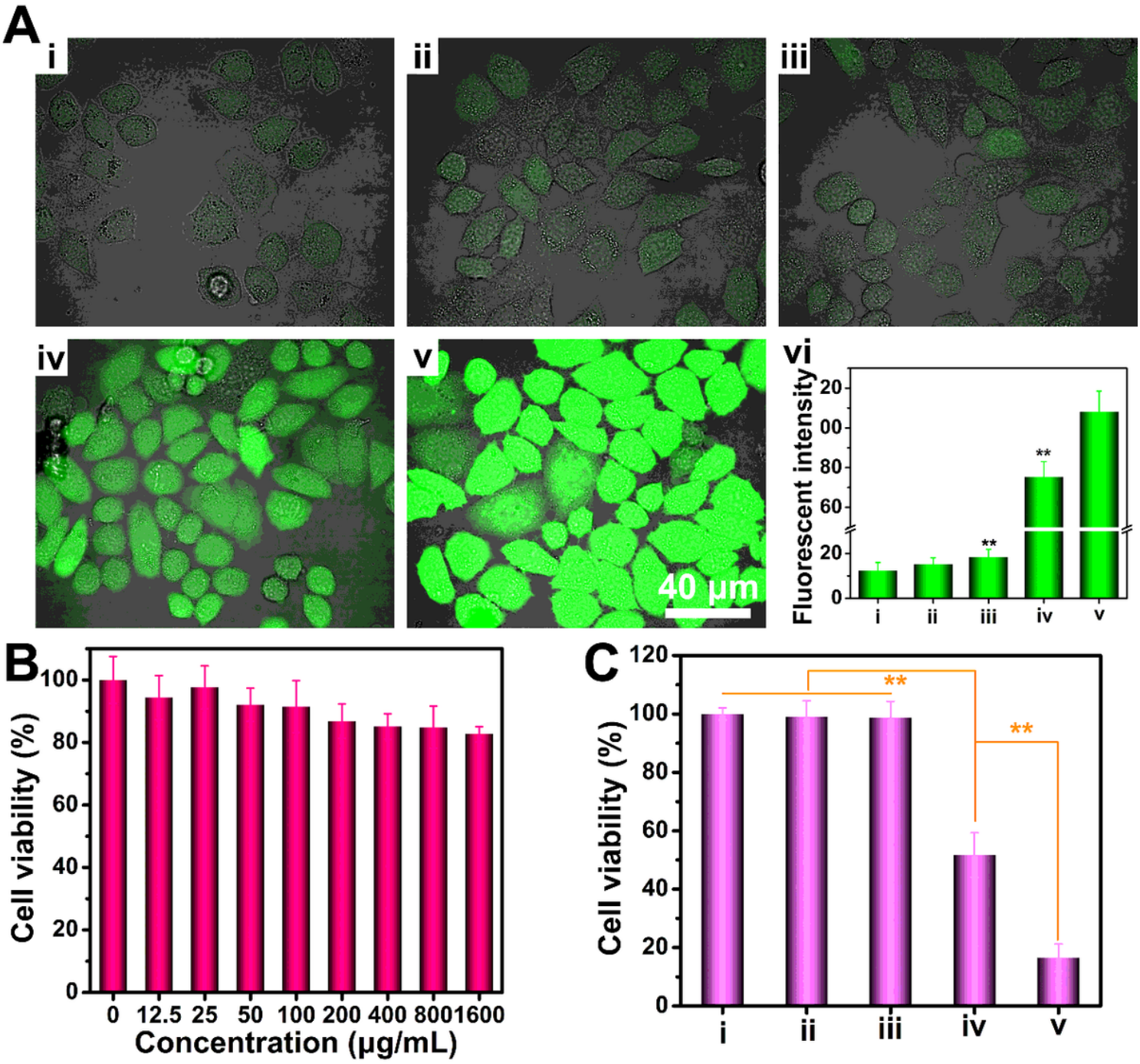

Figure 5

(A) CLSM images of DCFH-DA stained PC-3 cells after treated with (i) complete culture medium, (ii) NIR laser irradiation, (iii) ICG@FeDH alone, (iv) ICG@FeD plus laser irradiation and (v) targeted ICG@FeDH plus laser irradiation. And (vi) The mean fluorescence determined from the corresponded CLSM images. (B) Cell viability of PC-3 cells incubated with FeDH at different concentrations for 24 h. (C) Cell viability of PC-3 cells subjected to the corresponding treatments: (i) complete culture medium, (ii) NIR laser irradiation, (iii) ICG@FeDH alone, (iv) ICG@FeD plus laser irradiation and (v) targeted ICG@FeDH plus laser irradiation.

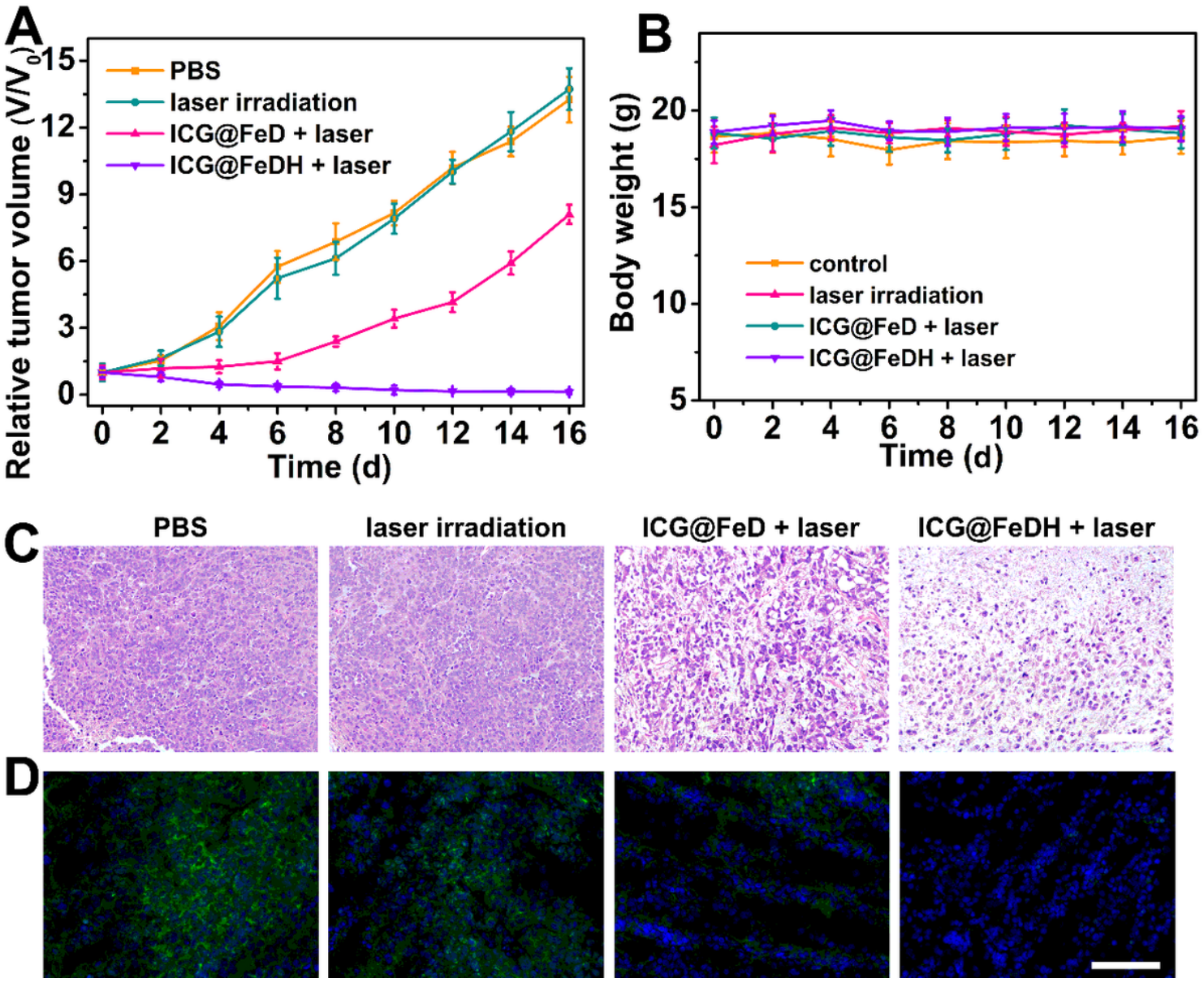

Figure 6

(A) The change of relative tumor volume within two weeks under different treatments. (B) The change of body weights of experimental mice of different groups in the period of treatments. (C) H&E staining and (D) Immunofluorescence staining for HIF-1α expression level of histological sections from tumor tissues in different groups. Green color in D represents HIF-1α and Blue color represents DAPI. Scale bar in C and D is 200 μm.

Supplementary Files

This is a list of supplementary files associated with this preprint. Click to download.

- Onlinefloatimage1.Png